https://doi.org/10.5194/egusphere-2025-5064
Preprint. Discussion started: 14 November 2025

Exploring the processes of liquid water path sensitivity to aerosol-cloud interactions using output from a high-resolution large-eddy simulation

Sudhakar Dipu[1], Johannes Mülmenstädt[1,2], and Johannes Quaas[1]

[1]Institute for Meteorology, Universität Leipzig, Leipzig, Germany
[2]now at: Pacific Northwest National Laboratory, Richland, USA

Correspondence: Sudhakar Dipu (dipu.sudhakat@uni-leipzig.de)

Abstract. Diagnostics from high-resolution Large-Eddy Simulations (LES) are used to investigate aerosol impacts on the liquid water path (LWP) sensitivity in a non-precipitating, single-layer liquid cloud regime. In two LES simulations, the 2013 conditions represent a low aerosol scenario, while the 1985 conditions represent a high aerosol scenario. Joint histograms of cloud droplet number concentration (N_d) and LWP reveal a non-linear relationship, with positive LWP sensitivity (increasing LWP with N_d) at low Nd and negative sensitivity at high N_d. The transition from positive to negative LWP sensitivity occurs at higher N_d values in the 1985 simulation ($\approx 300\,cm^{-3}$) compared to the 2013 simulation ($\approx 100\,cm^{-3}$), indicating that enhanced aerosol loading shifts the transition point. This shift reflects stronger droplet activation and sustained LWP growth under high CCN conditions. Diagnostics of the cloud dilution ratio indicate that negative LWP sensitivity is linked to enhanced cloud-top entrainment. The temporal evolution of the N_d–LWP relationship confirms increasing dominance of negative sensitivity in the 2013 case, while the 1985 case exhibits weaker LWP depletion. Additionally, aerosol perturbations also influence thermodynamic properties such as the apparent heating/cooling (Q_1) and the moisture sink (Q_2). Specifically, stronger cloud-top heating and moisture sinks are simulated during negative LWP sensitivity phases, particularly for high N_d in 2013, consistent with enhanced evaporation and entrainment. Aerosol perturbations thus modulate both microphysical and thermodynamic processes, producing distinct LWP sensitivity regimes with important implications for understanding aerosol–cloud–climate interactions.

1 Introduction

The aerosol cloud interactions (ACI) and the resulting effective radiative forcing remain a large source of uncertainty when assessing anthropogenic climate change (Forster et al., 2021; Quaas et al., 2020b). The uncertainty in ACI stems from the response of the clouds to the aerosol perturbation (Forster et al., 2020). In liquid clouds, cloud droplets form on an aerosol particle, which can serves as cloud condensation nucleus (Charlson et al., 1992). An increase in atmospheric aerosol leads to an increase in the cloud droplet number concentration (N_d). Twomey (1974) hypothesised that at a constant liquid water path (LWP), an increased aerosol burden leads to clouds with more numerous small droplets, which increase the cloud albedo. In addition, smaller droplets delay the precipitation formation by reducing the collision–coalescence efficiency and increasing

https://doi.org/10.5194/egusphere-2025-5064
Preprint. Discussion started: 14 November 2025

the cloud lifetime (Albrecht, 1989). The increase in the response in the N_d also leads to further rapid adjustment of the cloud properties. It includes the alteration of cloud drop size distribution, changes in the LWP, cloud fraction, and dynamic process (Ackerman et al., 2000; Mülmenstädt and Feingold, 2018). Thus, the instantaneous Twomey effect and cloud rapid adjustments contribute to the effective radiative forcing due to ACI (Bellouin et al., 2020; Quaas et al., 2024).

The response of cloud water path, the vertical integral of cloud water, to aerosol perturbation is a key component of cloud adjustments, and yet it is uncertain. This is particularly because of the elusive sign of the LWP adjustment/sensitivity to aerosol perturbations and its regime dependency (Fons et al., 2023; Dipu et al., 2022; Glassmeier et al., 2021; Possner et al., 2020; Gryspeerdt et al., 2019). A positive LWP adjustment is mainly observed in precipitating clouds, in which an increase in the aerosol results in enhanced N_d and smaller droplets, suppressing the precipitation and allowing for an accumulation of LWP (Albrecht, 1989). Thus, the positive LWP adjustment results in thicker and more reflective clouds with a stronger cooling effect. On the other hand, a negative LWP adjustment is associated with cloud droplet evaporation. The numerous small droplets also lead to droplet sedimentation and enhance radiative cooling at the cloud top, which can initiate turbulence and entrainment of warm, dry air into the cloud. Further, the entrainment of warm, dry air into the cloud leads to evaporation of the smaller droplets, resulting in decreases in LWP or negative LWP adjustment (Williams and Igel, 2021; Bretherton et al., 2007; Ackerman et al., 2004; Wang et al., 2003). Both observational and modelling studies demonstrate a strong offsetting warming effect from negative LWP adjustment (Gryspeerdt et al., 2021; Possner et al., 2020). However, the strength of the net LWP adjustment is modulated by the environmental condition. As a net result of the opposing LWP adjustment mechanisms, their net impact on the large-scale integral remains relatively small or neutral (Zhang et al., 2022). Thus, the bidirectional LWP adjustment/sensitivity, precipitation suppression, and droplet evaporations are difficult to disentangle as these processes coexist in the cloud (Fons et al., 2023).

Recent studies have focused on the sensitivity of LWP to N_d to quantify the impact of aerosols on LWP, (Dipu et al., 2022; Gryspeerdt et al., 2019; Bellouin et al., 2020). Using satellite observations, Gryspeerdt et al. (2019) demonstrated that the LWP-N_d relation is non-linear over the global ocean. The LWP adjustment is also regime-dependent (Glassmeier et al., 2021). In marine stratocumulus clouds, the Nd-LWP relationship is non-linear, and the co-variability between LWP and N_d primarily drives it (Goren et al., 2024). The LWP adjustment estimated based on satellite observations may be highly uncertain and negatively biased (Arola et al., 2022) because of the retrieval errors and also due to correlated errors in the N_d and LWP retrievals (Quaas et al., 2020a; Gryspeerdt et al., 2019; Grosvenor et al., 2018) In contrast, modelling studies often reported positive LWP adjustments (Quaas et al., 2008; Gryspeerdt et al., 2020). However, modelling evidence has also shown negative LWP adjustment, in which the altered N_d leads to entrainment mixing, thereby reducing the LWP (Glassmeier et al., 2021; Ackerman et al., 2004). Mülmenstädt et al. (2024b) reported that the latest generation of general circulation models (GCMs) are able to produce negative LWP adjustment besides positive LWP adjustment through precipitation suppression in response to increased N_d. However, the earlier-generation GCMs fail to show negative LWP adjustments in response to anthropogenic aerosols.

https://doi.org/10.5194/egusphere-2025-5064
Preprint. Discussion started: 14 November 2025

Previous studies focused on the LWP-N_d relationship to assist in understanding ACI. Observational studies use natural events where the aerosol perturbation is known and compared with unperturbed cloud regimes (Christensen et al., 2022). Such studies suggest an unchanged LWP or negative LWP adjustment (Malavelle et al., 2017; Toll et al., 2019); however, such cases are limited. Modelling studies, specifically high-resolution LES simulations, are ideal for improving the understanding of the LWP adjustment by varying aerosol concentration while keeping the other boundary conditions constant. However, the LES simulations are computationally expensive, and the simulations are regime-dependent. Most of the previous LES studies suggest that a positive LWP adjustment is associated with precipitating cloud regimes and a negative LWP adjustment is simulated for non-precipitating cloud regimes (Glassmeier et al., 2021; Ackerman et al., 2004; Hill et al., 2009; Lee et al., 2009; Wang et al., 2011). In this study, we aim to investigate the LWP sensitivity in a non-precipitating continental cloud regime using high-resolution LES model simulation in numerical weather prediction mode, with initial and boundary conditions for a real weather situation, and with interactive land surface (Heinze et al., 2017; Costa-Surós et al., 2020). This LES simulates bidirectional LWP sensitivity (Dipu et al., 2022). Using the perturbed aerosol simulation of the same cloud regime, here we investigate the impact of aerosol on bidirectional LWP sensitivity. This allows us to infer to which degree the LWP-Nd relationship represents a causal influence of Nd on LWP. We examine the impact of aerosol on positive and negative LWP sensitivity and investigate the microphysical and thermodynamic processes controlling the sign and magnitude of LWP sensitivity.

2 Data and Methodology

Large-eddy simulations (LES) using the ICOsahedral Nonhydrostatic (ICON) model (Dipankar et al., 2015; Zängl et al., 2015) are analysed in this study. The atmospheric model ICON has been configured to a large-eddy simulation framework (Dipankar et al., 2015), and has been evaluated against standard LES models and multiple observations (Heinze et al., 2017). The high resolution, ICON-LES simulation has been performed as part of the High Definition Clouds and Precipitation for advancing Climate Prediction (HD(CP)^2) project. The simulation ran over a large domain (over Germany) in a weather prediction mode, which uses realistic boundary conditions from the operational COSMOS-DE (Consortium for Small Scale Modelling, Baldauf et al., 2011), with a fully interactive land surface (Costa-Surós et al., 2020). The model is configured with a horizontal resolution of 156 m and 150 vertical levels with a model top at 21 km. A sub-grid scale turbulence scheme based on the classical Smagorinsky scheme is used in the model, which also accounts for thermal stratification (Lilly, 1962). The model uses a two-moment liquid and ice-phase bulk microphysics scheme (Seifert and Beheng, 2006). The CCN concentrations in the model are prescribed as a spatially and temporally varying distribution. The control simulation uses CCN concentrations as estimated for 02 May 2013 (Costa-Surós et al., 2020)., and for the perturbed simulation, CCN concentrations valid for the year approximately 1985 were selected, in which the pollution level in Europe was at its peak (Smith et al., 2011). The simulations were performed over Germany for selected dates, of which the date 02 May 2013 is considered in the study based on the evaluation results from Heinze et al. (2017). The 02 May 2023 has been one of the extensive measurement campaigns for the HD(CP)^2 Observational Prototype Experiment (HOPE, Löhnert et al., 2015; Madhavan et al., 2016) and the evaluation results from Heinze et al. (2017) suggest the presence of a wide range of cloud regimes, compared to other HD(CP)^2 simulations. A

https://doi.org/10.5194/egusphere-2025-5064
Preprint. Discussion started: 14 November 2025

detailed description of the ICON-LES model and HD(CP)^2 simulations can be obtained from Dipankar et al. (2015), Heinze et al. (2017), and Costa-Surós et al. (2020).

Here, we have used the coarse-gridded data with a resolution of 1.2 km (grid size of 589 × 637); the actual ICON-LES simulation was performed with 156 m horizontal resolution, though. Five-minute instantaneous model output from 1000 hrs to 2000 hrs is considered for the study. The analysis is restricted to single-layered liquid clouds by excluding the clouds with a cloud-top temperature of less than 268 K. Further, for the analysis, we have considered cloud-top microphysical properties. The cloud top is defined as the topmost level with $N_d > 2$ cm^{-3}, which is further filtered for cloud fractions equal to 1 (at the 1.2 km scale) and cloud optical thicknesses greater than 2. Because of the high model resolution and high frequency of model output, the N_d is divided into logarithmic bin sizes of 1000 numbers. The corresponding bin mean cloud microphysical properties are used for the analysis. Additionally, to quantify the grid scale impact of aerosol, cloud properties at the same grid points for both simulations are considered, assuming that the initialization of the cloud fields leads to approximately in the same location in both simulations.

The apparent heating (Q_1) and the moisture sink (Q_2) at the cloud top are calculated by following Yanai et al. (1973). Q_1 represents the apparent heating/cooling of the atmospheric layer due to various processes such as radiation, condensation, and convection. The corresponding equation is given by,

$$Q_1 = c_p \frac{\partial T}{\partial t} - c_p(\omega\sigma - V \cdot \nabla T) \tag{1}$$

where, $\sigma = \left(\frac{RT}{c_p P}\right) - \left(\frac{\partial T}{\partial p}\right)$, the static stability, p is the pressure, V is the horizontal velocity vector, ∇ horizontal gradient operator, c_p is the specific heat of dry air at constant pressure, T is the temperature, ω is the vertical p velocity, and t is the time. Additionally, Q_2 represents the drying/moistening due to condensation or evaporation and moisture flux convergence, and it is represented as,

$$Q_2 = -L\frac{\partial q}{\partial t} - LV \cdot \nabla q - L\omega\frac{\partial q}{\partial t} \tag{2}$$

where q is the specific humidity. The cloud dilution ratio, which serves as a proxy for entrainment, is defined as the ratio of the cloud effective radius to the adiabatic radius. The latter is approximated by following Brenguier et al. (2000), which is given by

$$R_{\text{ad}} \approx \left(\frac{3LWC}{4\pi\rho_w N_d}\right)^{\frac{1}{3}} \tag{3}$$

Where, LWC is liquid water content (g/m^2), N_d is the cloud droplet number concentration (cm^{-3}), and ρ_w is water density (kg/m^{-3}). The joint histograms analyzed in this study are constructed as conditional probabilities (CP [%]) following Gryspeerdt et al. (2016) and are defined as the probability of finding a certain LWP given that a certain N_d has been observed (CP = [P (LWP | N_d) × 100%]). For joint histogram analysis, the variables are binned with a bin size of 1000. In the following analysis, N_d-bin mean variables are used, which means $\overline{\text{variable}}$ at certain N_d bins (P (variable | N_d)).

https://doi.org/10.5194/egusphere-2025-5064
Preprint. Discussion started: 14 November 2025

2.1 Results

The aerosol perturbation in the 1985 simulations results in a significant increase in the number of cloud droplets, as demonstrated by the shift in the N_d probability density function (PDF) distribution (Fig. 1a) towards higher N_d. In 2013, the N_d is primarily distributed between 2 and 700 cm^{-3}. In contrast, the 1985 simulation shows a broader distribution that extends up to 1000 cm^{-3}, suggesting greater activation of N_d due to aerosol perturbation. Furthermore, this perturbation results in a 120% increase in the mean N_d compared to the 2013 simulation. However, the LWP distribution shows relatively small shifts towards higher LWP in the 1985 simulation compared to 2013 (Fig. 1b). The relatively small shift in 1985 indicates that aerosol perturbation has less impact on the LWP, contributing only to a 5% increase in the mean LWP when compared to the 2013 simulation. The contrasting response of the N_d and LWP to the aerosol perturbation suggests that higher droplet activation alone does not directly translate into proportional increases in bulk water content, pointing to the role of additional microphysical and dynamical processes (e.g., entrainment and/or dilution).

To disentangle these processes, we have extended the analysis to the joint histogram of LWP and N_d. Fig. 2 shows the joint histogram between LWP and N_d for the 1985 and 2013 simulations. In both cases, the maximum condition probability (CP) depicts a spread for LWP values ranging from 10 to 500 gm^{-2}, particularly at low N_d ($< 100\,cm^{-3}$). At the middle N_d values (between 100 and 500 cm^{-3}), the CP narrows, with the highest values occurring in this range for both simulations. At higher N_d, the CP spread increases further, especially in 2013, though CP values above 700 cm^{-3} remain low. This low CP shows that there are limited cloud regimes with high N_d in the 2013 simulation. It is also evident in the N_d distribution (probability density function, PDF) shown in Fig. 1a.

The N_d-bin mean LWP ($\overline{LWP}$) in the joint histogram implies the tendency of the N_d-LWP relation. For both simulations, the $\overline{LWP}$ shows a non-linear relationship consistent with prior studies (Gryspeerdt et al., 2019; Dipu et al., 2022). This non-linear relation implies a positive LWP sensitivity ($\overline{LWP}$ increasing with N_d) for lower N_d values and a negative LWP sensitivity ($\overline{LWP}$ decreases with increasing N_d) for higher N_d values. The transition point where the positive LWP sensitivity shifts to negative varies with the aerosol perturbation. In the 2013 simulation, the transition from positive to negative LWP sensitivity is simulated around $N_d \approx 100\,cm^{-3}$ and in the 1985 simulation, it shifts to $N_d \approx 300\,cm^{-3}$. This shift reflects the impact of elevated CCN concentrations in 1985, which sustained droplet activation and delayed LWP depletion. The effect of aerosol perturbation is also evident in the R_{eff}. In the 2013 simulation, $\overline{R_{eff}}$ peaks at low N_d and then declines sharply beyond ≈ 100 cm^{-3} indicating stronger cloud depletion. Conversely, in the 1985 simulation, the $\overline{R_{eff}}$ decreases at larger $N_d \approx 300$ cm^{-3} indicating thicker, less diluted clouds (figure not shown). The cloud dilution ratio, which is defined as the ratio of $\overline{R_{eff}}$ to the adiabatic $\overline{R_{ad}}$ serves as a proxy for entrainment mixing. Values close to 1 indicate adiabatic clouds, while lower values suggest dilution. Fig. 3 shows the relation between N_d and the dilution ratio. For positive LWP sensitivity, the cloud dilution ratio increases (clouds become more adiabatic), and for negative LWP sensitivity, the dilution ratio tends to decrease, indicating a less adiabatic cloud regime or cloud dilution in both simulations. In particular, for the negative LWP sensitivity, the decrease in the dilution ratio is more prominent, with a substantial reduction in the LWP for the 2013 simulation. However, in the 1985 simulation, despite the reduction in the dilution rate for negative LWP sensitivity, the aerosol perturbation leads to thicker clouds with higher LWP,

https://doi.org/10.5194/egusphere-2025-5064
Preprint. Discussion started: 14 November 2025

which experience a lower dilution ratio, indicating a relatively more adiabatic state. In contrast, the 2013 simulation shows thinner clouds that are more diluted (characterized by a lower dilution ratio compared to 1985) or less adiabatic, highlighting a significant effect of entrainment at higher N_d.

Furthermore, the temporal evolution of the cloud field in both simulations illustrates time-dependent LWP sensitivity during the simulations. Fig. 4 illustrates the temporal evolution of the LWP sensitivity (time evolution of the joint histogram between LWP and N_d) for both simulations. Initially, both simulations exhibit positive LWP sensitivity. Over time, however, the relationship becomes more non-linear, with an increasing contribution from negative sensitivity. In the 1985 simulation, the positive LWP sensitivity dominates due to the high CCN concentration, which accounts for the activation of numerous smaller droplets. Additionally, the transition of positive to negative LWP sensitivity shifts toward a much higher N_d value in the 1985 simulation over time. Glassmeier et al. (2021) reported that the LWP sensitivity becomes increasingly negative over time in stratocumulus clouds. Likewise, the LWP sensitivity becomes more negative in both simulations over time. The numerical value of the negative LWP sensitivity is derived as the slope of the linear regression through the $\overline{LWP}$ in the specific N_d-bins, depicted in Fig. 5. Notably, the 2013 simulation exhibits a stronger negative slope than 1985, highlighting more rapid LWP depletion. Although the transition point of the negative LWP sensitivity shifts towards higher N_d in 1985, the numerical value of the LWP sensitivity (negative slope) is smaller compared to the 2013 simulation over time.

Fig. 6 further illustrates the critical $\overline{N_d}$ and corresponding $\overline{R_{eff}}$ at the transition between positive and negative LWP sensitivity. In the 2013 simulation, the critical $\overline{N_d}$ is mostly distributed between 48 and 490 cm^{-3}, with maximum density centred around 100 to 200 cm^{-3}, whereas in 1985, it ranges from 140 to 711 cm^{-3}, with the maximum density centred around 400 cm^{-3} in the 1985 simulation. This confirms the rightward shift in the LWP transition point under high-aerosol conditions. At this critical $\overline{N_d}$, $\overline{R_{eff}}$ shows a relatively widespread distribution, between 4.7 and 8 μm , in the 2013 simulation. Meanwhile, the 1985 simulation shows a relatively small spread in the $\overline{R_{eff}}$ distribution, between 4.2 and 6.5 μm further reflecting more variable cloud dilution in the low-aerosol case.

Further insights into aerosol-induced cloud changes are revealed by analyzing thermodynamic diagnostics, particularly the apparent heating (Q_1) and moisture sink (Q_2) at the cloud top. The Q_1 in a cloud layer is associated with various processes, local temperature changes, advection, and vertical motion. A substantial part of apparent heating/cooling is also associated with cloud microphysical processes in clouds. In liquid clouds, condensation of water vapour contributes to microphysical heating, and cloud droplet evaporation contributes to cooling (Keshtgar et al., 2023). Fig. 7 a shows the relationship between $\overline{Q_1}$ (N_d-bin mean) and N_d at the cloud top. For lower N_d values, the $\overline{Q_1}$ is negative, implying apparent cooling in both simulations. A negative $\overline{Q_1}$ is mainly associated with cloud droplet evaporation, rising motion and cold air advection in a cloudy layer. Specifically, in the selected case, at lower N_d, the $\overline{Q_1}$ is negative, though it becomes less negative as N_d increases. The negative $\overline{Q_1}$ observed at lower N_d may be related to processes such as droplet evaporation and/or rising motion. As the cloud develops, the $\overline{R_{eff}}$ increases due to greater collision efficiency, which in turn reduces droplet evaporation and results in a less negative $\overline{Q_1}$ as

https://doi.org/10.5194/egusphere-2025-5064
Preprint. Discussion started: 14 November 2025

N_d increases. This is consistent with concurrent increases in LWC and decreases in specific humidity at lower N_d (Fig. S2). In the 2013 simulation, as N_d increases ($> 200\ cm^{-3}$), $\overline{Q_1}$ becomes positive, indicating apparent heating. However, this apparent heating is only simulated at higher N_d ($> 800\ cm^{-3}$) in the 1985 simulation. A positive $\overline{Q_1}$ is associated with processes such as condensation and latent heat release, sinking motion, and warm air advection. In the 2013 simulation, however, the specific humidity increases, and the water content (LWC/LWP) decreases as $N_d > 200\,cm^{-3}$. Therefore, the only possible mechanism left to explain the positive $\overline{Q_1}$ is the warm air advection and the resulting cloud droplet evaporation, which is in agreement with the dilution of clouds with higher N_d (Fig. 3). Similarly, in the 1985 simulation, the negative $\overline{Q_1}$ further decreases (less negative) for higher N_d ($> 300\,cm^{-3}$) and a positive $\overline{Q_1}$ is simulated only at higher N_d ($> 800\,cm^{-3}$), suggesting that aerosol perturbation shifts the onset of entrainment-induced cloud depletion to higher N_d.

The apparent moisture sink, Q_2 (N_d-bin mean, $\overline{Q_2}$), for the two simulations is depicted in Fig. 7b, which also supports the above interpretation. Generally, a positive Q_2 indicates moisture removal through condensation or dry air advection, while a negative Q_2 implies moisture addition through evaporation or moist air advection. In the 2013 simulation, $\overline{Q_2}$ is negative for the lower N_d ($< 100\,cm^{-3}$), indicating the dominant influence of moist air advection, along with cloud dilution. Simultaneously, the $\overline{Q_2}$ increases as N_d increases for lower N_d, suggesting a reduction in cloud dilution, which correlates with an increase in LWC and a decrease in specific humidity (Fig. A1). In contrast, for higher ($N_d > 100\ cm^{-3}$), in the 2013 simulation, $\overline{Q_2}$ tends to be positive, indicating moisture removal—consistent with entrainment-driven evaporation. The 1985 simulation shows predominantly positive $\overline{Q_2}$, except for very low N_d ($> 10\,cm^{-3}$). The positive $\overline{Q_2}$ for N_d values less than $300\,cm^{-3}$ is driven by condensation. At higher N_d ($> 300\,cm^{-3}$), however, the same positive $\overline{Q_2}$ results from cloud water removal through dry air entrainment. This is also consistent with a concurrent increase in the specific humidity and the decrease in LWC, indicating cloud dilution associated with entrainment.

3 Discussion

The ambiguity in the LWP adjustment/sensitivity due to aerosols varies with individual clouds (Smalley et al., 2024; Christensen et al., 2020), which adds uncertainty to effective radiative forcing due to the aerosol-cloud interactions (Mülmenstädt and Feingold, 2018). Recent studies utilise the sensitivity of N_d to LWP to improve the understanding of the aerosol-cloud interaction using modelling and observations (Gryspeerdt et al., 2019; Dipu et al., 2022; Mülmenstädt et al., 2024a), in which N_d represents an indirect proxy for aerosols. In a specific cloud regime, a positive LWP sensitivity implies a systematic increase of LWP with increasing aerosols, and a negative LWP sensitivity indicates cloud depletion. Here, we have investigated the significance of aerosol perturbation to the LWP sensitivity using the ICON-LES model.

In the selected cloud regime, the 1985 simulation, representing a high-aerosol scenario, consistently showed systematically higher N_d values under identical meteorological conditions compared to the 2013 simulation (low-aerosol scenario). The high CCN in the 1985 simulation led to more numerous and smaller droplets, sustaining positive LWP sensitivity compared to 2013.

https://doi.org/10.5194/egusphere-2025-5064
Preprint. Discussion started: 14 November 2025

As a result, the transition point from positive to negative to positive LWP sensitivity has shifted to a higher N_d (>300 cm^{-3}), compared to that (>100 cm^{-3}) in 2013. This shift in the negative LWP sensitivity is also visible in the time evolution of the LWP sensitivity in the respective simulation. Despite this shift, both simulations exhibited negative LWP sensitivity at higher N_d, linked to cloud dilution due to entrainment. Analysis of the thermodynamic diagnostics further reveals that in both simulations, cloud-top Q_1 (apparent heating) and Q_2 (moisture sink) became increasingly positive with N_d, indicating warm, dry air entrainment and associated evaporation. The positive trend is more pronounced in 2013, consistent with stronger dilution. Meanwhile, in 1985, Q_1 and Q_2 remained less positive, suggesting a more buffered response to entrainment due to sustained cloud development under high aerosol loading. Additional diagnostics of the temperature tendency term in Q_1 (eq. 1) at cloud top reveal that it becomes increasingly negative as N_d increases, particularly for negative LWP sensitivity (Fig. A2 a). The positive advection terms (the sum of horizontal and vertical advection) in Q_1 (eq. 1) for low N_d indicating net warming due to advection, which later transitioned to neutral or negative values at higher N_d, indicating reduced warming and as entrainment increases (Fig. A2 c). The high CCN in the 1985 simulations resulted in a less negative temperature tendency (less cooling) and advection-induced cooling compared to the 2013 simulation. Similarly, specific humidity tendencies term in Q_2 (eq. 2) also showed increased moisture loss at higher N_d, particularly in 2013, further confirming the role of entrainment-driven drying. In the 2013 case, net moisture advection term in Q_2 (eq. 2) is initially positive at lower N_d, and it becomes negative at higher N_d, consistent with entrainment-induced drying (Fig. A2 b). Conversely, in the 1985 simulation, net moisture advection remains persistently negative and intensifies slightly with increasing N_d, suggesting a weak drying tendency under high aerosol conditions (Fig. A2 d).

The analysis clearly indicates that aerosol perturbations and aerosol levels have a significant impact on the LWP sensitivity and associated processes. In the 2013 simulation, Q_1 becomes less negative and positive for negative LWP sensitivity (N_d > 100 cm^{-3}). The observed positive tendency in Q_1 for negative LWP sensitivity could be due to warm entrainment, which leads to evaporation of cloud droplets. Moreover, this evaporation, along with a decrease in local specific humidity, contributes to a moisture sink ($Q_2 > 0$), particularly for negative LWP sensitivity. However, in the 1985 simulation, aerosol perturbations led to a less positive tendency in Q_2 for negative LWP sensitivity compared to prior simulations. This can be further explained by the weaker temperature tendencies, reduced local specific humidity, and decreased moisture sink in the 1985 simulation for negative LWP sensitivity. Furthermore, in the 1985 simulation, condensation processes dominate (positive Q_2), which helps maintain a positive LWP sensitivity even at higher N_d. Nonetheless, as N_d increases further, Q_2 also increases, which may be due to enhanced droplet evaporation linked to warm air entrainment. It should be emphasised, however, that evaporation and advection are not the only processes associated with negative LWP sensitivity. While they appear to be the dominant mechanisms in the above simulations, additional processes such as cloud-top radiative cooling, droplet sedimentation, and turbulence entrainment feedbacks may also play important roles in driving cloud depletion at high N_d. Future studies should aim to disentangle and quantify the relative contributions of these pathways, for example, by combining targeted LES experiments with process-level diagnostics and Lagrangian cloud tracking.

https://doi.org/10.5194/egusphere-2025-5064
Preprint. Discussion started: 14 November 2025

4 Conclusions

This study uses the ICON-LES model as part of the HD(CP)2 project to investigate the effect of aerosols on LWP sensitivity. Simulations were conducted over Germany on May 2, 2013, with high (1985 CCN condition) and low aerosol (2013 CCN condition) scenarios. The joint histogram analysis reveals a non-linear relationship between N_d and LWP in both simulations, which is consistent with previous studies. The non-linear relationship implies for low N_d values, LWP increases with N_d (positive LWP sensitivity), while at higher N_d, LWP decreases (negative LWP sensitivity). The transition from positive to negative LWP sensitivity occurs at a lower N_d ($\approx 100\,cm^{-3}$) in the 2013 simulation and shifts to higher N_d ($\approx 300\,cm^{-3}$) under the 1985 aerosol scenario. This indicates that increased aerosol concentration leads to sustained droplet activation, thereby shifting the cloud depletion to higher N_d. The 1985 simulation exhibits more persistent positive LWP sensitivity, associated with enhanced droplet activation and thicker clouds. In contrast, the 2013 simulation reveals a greater degree of cloud dilution, as indicated by a more pronounced decrease in the R_{eff} and dilution ratio at higher N_d. Temporal analysis of the N_d-LWP joint histogram further illustrates a non-linear relationship with negative LWP sensitivity becomes dominant over time in 2013. However, in the 1985 simulation, positive LWP sensitivity is dominant, with weaker negative LWP sensitivity observed over time.

Furthermore, the thermodynamic features such as cloud top apparent heating (Q_1) and moisture sink (Q_2) also reveal a significant impact of aerosol perturbation. Our analysis suggests that negative Q_1 dominates at low N_d, due to droplet evaporation and/or rising motion. In contrast, the apparent heating (positive Q_1) observed at higher N_d is attributed to cloud dilution and warm air advection. In the 2013 simulation, we found apparent heating or positive Q_1 for $N_d > 200\,cm^{-3}$. In contrast, the 1985 simulation showed positive Q_1 only at a much higher N_d value ($> 800\,cm^{-3}$). Thus, the aerosol perturbation results in sustained negative Q_1 for higher N_d, with a weaker positive Q_1 or cloud dilution through entrainment. Similarly, negative Q_2 or moisture gain is simulated at low N_d despite the negative Q_1, indicating dominant cloud growth. While positive Q_2 or moisture sink is simulated at higher N_d, indicating a drying effect through warm air entrainment. Our analysis suggests that high CCN concentration in the 1985 simulation exhibits greater moisture retention (negative Q_2), supporting sustained cloud growth and positive LWP sensitivity to higher N_d. In contrast, the moisture sink (positive Q_2) is observed in relatively higher N_d ($> 800\,cm^{-3}$) in the 1985 simulation.

Both simulations reinforce the hypotheses that negative LWP sensitivity at high N_d are closely associated with entrainment-driven cloud dilution, evidenced by increased Q_1 (warming), increased Q_2 (moisture loss), reduced LWC, and droplet evaporation. However, the threshold N_d for dilution shifts to higher N_d in the 1985 simulation, indicating the enhanced effect of aerosol perturbation on mitigating cloud depletion. The response in the N_d–LWP relationship under aerosol perturbations implies a modified cloud radiative response, with sustained positive LWP sensitivity enhancing cloud albedo towards high N_d with weaker cloud depletion through entrainment at higher N_d. These dynamics are critical for quantifying the effective radiative forcing of aerosol-cloud interactions in convective cloud regimes. Future studies will focus on investigating N_d-LWP sensitivity and its effect on aerosol perturbation using Lagrangian cloud tracking, which can improve the understanding of the

https://doi.org/10.5194/egusphere-2025-5064
Preprint. Discussion started: 14 November 2025

aerosol effect on LWP sensitivity.

Data availability. The model output data used for the development of the research in the frame of this scientific article is securely saved in the tape archives at the Deutsches Klimarechenzentrum (DKRZ), which will be accessible for 10 years. Additionally, backup copies are stored in the University of Leipzig and University of Cologne backup services.

Author contributions. All authors participated in the design of the study. DS & JQ conceived and refined the overall structure of the investigation based on discussions with and feedback from all co-authors. All authors assisted in the interpretation of the results and commented on the paper. All authors have read and agreed to the published version of the manuscript.

Competing interests. Some authors are members of the editorial board of the journal Atmospheric Chemistry and Physics.

Acknowledgements. This study has been carried out under the project "FORCeS", which is funded by the European Union's Horizon 2020 research and innovation programme under grant agreement No 821205. Further funding from the DFG-ANR project "CDNC4aci" (Deutsche Forschungsgemeinschaft, DFG GZ QU 311/27-1) is acknowledged. We thank the High Definition Clouds and Precipitationfor Advancing Climate Prediction (HD(CP)2) project (funded by the German Federal Ministry of Education and Research (BMBF; http://www.fona.de/) under grant no. 01LK1504B) for providing the model simulations. EG was supported by a Royal Society University Research Fellowship (URF/R1/191602).

https://doi.org/10.5194/egusphere-2025-5064
Preprint. Discussion started: 14 November 2025

References

Ackerman, A. S., Toon, O. B., Taylor, J. P., Johnson, D. W., Hobbs, P. V., and Ferek, R. J.: Effects of Aerosols on Cloud Albedo: Evaluation of Twomey's Parameterization of Cloud Susceptibility Using Measurements of Ship Tracks, Journal of the Atmospheric Sciences, 57, 2684 – 2695, https://doi.org/10.1175/1520-0469(2000)057<2684:EOAOCA>2.0.CO;2, 2000.

Ackerman, A. S., Kirkpatrick, M. P., Stevens, D. E., and Toon, O. B.: The impact of humidity above stratiform clouds on indirect aerosol climate forcing, Nature, 432, 1014–1017, https://doi.org/10.1038/nature03174, 2004.

Albrecht, B. A.: Aerosols, Cloud Microphysics, and Fractional Cloudiness, Science, 245, 1227–1230, https://doi.org/10.1126/science.245.4923.1227, 1989.

Arola, A., Lipponen, A., Kolmonen, P., Virtanen, T. H., Bellouin, N., Grosvenor, D. P., Gryspeerdt, E., Quaas, J., and Kokkola, H.: Aerosol effects on clouds are concealed by natural cloud heterogeneity and satellite retrieval errors, Nature Communications, 13, 7357, https://doi.org/10.1038/s41467-022-34948-5, 2022.

Baldauf, M., Seifert, A., Förstner, J., Majewski, D., Raschendorfer, M., and Reinhardt, T.: Operational Convective-Scale Numerical Weather Prediction with the COSMO Model: Description and Sensitivities, Mon. Weather Rev., 139, 3887–3905, https://doi.org/10.1175/MWR-D-10-05013.1, 2011.

Bellouin, N., Quaas, J., Gryspeerdt, E., Kinne, S., Stier, P., Watson-Parris, D., Boucher, O., Carslaw, K., Christensen, M., Daniau, A.-L., Dufresne, J.-L., Feingold, G., Fiedler, S., Forster, P., Gettelman, A., Haywood, J. M., Lohmann, U., Malavelle, F., Mauritsen, T., McCoy, D., Myhre, G., Mülmenstädt, J., Neubauer, D., Possner, A., Rugenstein, M., Sato, Y., Schulz, M., Schwartz, S. E., Sourdeval, O., Storelvmo, T., Toll, V., Winker, D., and Stevens, B.: Bounding global aerosol radiative forcing of climate change, Rev. Geophys., 58, e2019RG000 660, https://doi.org/10.1029/2019RG000660, 2020.

Brenguier, J.-L., Pawlowska, H., Schüller, L., Preusker, R., Fischer, J., and Fouquart, Y.: Radiative Properties of Boundary Layer Clouds: Droplet Effective Radius versus Number Concentration, J. Atmos. Sci., 57, 803 – 821, https://doi.org/10.1175/1520-0469(2000)057<0803:RPOBLC>2.0.CO;2, 2000.

Bretherton, C. S., Blossey, P. N., and Uchida, J.: Cloud droplet sedimentation, entrainment efficiency, and subtropical stratocumulus albedo, Geophysical Research Letters, 34, https://doi.org/https://doi.org/10.1029/2006GL027648, 2007.

Charlson, R. J., Schwartz, S. E., Hales, J. M., Cess, R. D., Coakley, J. A., Hansen, J. E., and Hofmann, D. J.: Climate Forcing by Anthropogenic Aerosols, Science, 255, 423–430, https://doi.org/10.1126/science.255.5043.423, 1992.

Christensen, M. W., Jones, W. K., and Stier, P.: Aerosols enhance cloud lifetime and brightness along the stratus-to-cumulus transition, Proceedings of the National Academy of Sciences, 117, 17 591–17 598, https://doi.org/10.1073/pnas.1921231117, 2020.

Christensen, M. W., Gettelman, A., Cermak, J., Dagan, G., Diamond, M., Douglas, A., Feingold, G., Glassmeier, F., Goren, T., Grosvenor, D. P., Gryspeerdt, E., Kahn, R., Li, Z., Ma, P.-L., Malavelle, F., McCoy, I. L., McCoy, D. T., McFarquhar, G., Mülmenstädt, J., Pal, S., Possner, A., Povey, A., Quaas, J., Rosenfeld, D., Schmidt, A., Schrödner, R., Sorooshian, A., Stier, P., Toll, V., Watson-Parris, D., Wood, R., Yang, M., and Yuan, T.: Opportunistic experiments to constrain aerosol effective radiative forcing, Atmospheric Chemistry and Physics, 22, 641–674, https://doi.org/10.5194/acp-22-641-2022, 2022.

Costa-Surós, M., Sourdeval, O., Acquistapace, C., Baars, H., Carbajal Henken, C., Genz, C., Hesemann, J., Jimenez, C., König, M., Kretzschmar, J., Madenach, N., Meyer, C. I., Schrödner, R., Seifert, P., Senf, F., Brueck, M., Cioni, G., Engels, J. F., Fieg, K., Gorges, K., Heinze, R., Siligam, P. K., Burkhardt, U., Crewell, S., Hoose, C., Seifert, A., Tegen, I., and Quaas, J.: Detection and attribution of

https://doi.org/10.5194/egusphere-2025-5064
Preprint. Discussion started: 14 November 2025

aerosol–cloud interactions in large-domain large-eddy simulations with the ICOsahedral Non-hydrostatic model, Atmos. Chem. Phys., 20, 5657–5678, https://doi.org/10.5194/acp-20-5657-2020, 2020.

Dipankar, A., Stevens, B., Heinze, R., Moseley, C., Zïgl, G., Giorgetta, M., and Brdar, S.: Large eddy simulation using the general circulation model ICON, J. Adv. Model. Earth Syst., 7, 963–986, https://doi.org/https://doi.org/10.1002/2015MS000431, 2015.

Dipu, S., Schwarz, M., Ekman, A. M. L., Gryspeerdt, E., Goren, T., Sourdeval, O., Mülmenstädt, J., and Quaas, J.: Exploring Satellite-Derived Relationships between Cloud Droplet Number Concentration and Liquid Water Path Using a Large-Domain Large-Eddy Simulation, Tellus B: Chemical and Physical Meteorology, https://doi.org/10.16993/tellusb.27, 2022.

Fons, E., Runge, J., Neubauer, D., and Lohmann, U.: Stratocumulus adjustments to aerosol perturbations disentangled with a causal approach, npj Climate and Atmospheric Science, 6, 130, https://doi.org/10.1038/s41612-023-00452-w, 2023.

Forster, P., Storelvmo, T., Armour, K., Collins, W., Dufresne, J. L., Frame, D., Lunt, D., Mauritsen, T., Palmer, M., Watanabe, M., Wild, M., and Zhang, H.: The Earth's Energy Budget, Climate Feedbacks, and Climate Sensitivity, Cambridge University Press, chap, 7, 923–1054, 2021.

Forster, P. M., Forster, H. I., Evans, M. J., Gidden, M. J., Jones, C. D., Keller, C. A., Lamboll, R. D., Quéré, C. L., Rogelj, J., Rosen, D., Schleussner, C.-F., Richardson, T. B., Smith, C. J., and Turnock, S. T.: Current and future global climate impacts resulting from COVID-19, Nature Climate Change, 10, 913–919, https://doi.org/10.1038/s41558-020-0883-0, 2020.

Glassmeier, F., Hoffmann, F., Johnson, J. S., Yamaguchi, T., Carslaw, K. S., and Feingold, G.: Aerosol-cloud-climate cooling overestimated by ship-track data, Science, 371, 485–489, https://doi.org/10.1126/science.abd3980, 2021.

Goren, T., Chourdhury, G., Kretzschmar, J., and McCoy, I.: Co-variability drives the inverted-V sensitivity between liquid water path and droplet concentrations, EGUsphere, 2024, 1–18, https://doi.org/10.5194/egusphere-2024-2245, 2024.

Grosvenor, D. P., Sourdeval, O., Zuidema, P., Ackerman, A., Alexandrov, M. D., Bennartz, R., Boers, R., Cairns, B., Chiu, J. C., Christensen, M., Deneke, H., Diamond, M., Feingold, G., Fridlind, A., Hünerbein, A., Knist, C., Kollias, P., Marshak, A., McCoy, D., Merk, D., Painemal, D., Rausch, J., Rosenfeld, D., Russchenberg, H., Seifert, P., Sinclair, K., Stier, P., van Diedenhoven, B., Wendisch, M., Werner, F., Wood, R., Zhang, Z., and Quaas, J.: Remote Sensing of Droplet Number Concentration in Warm Clouds: A Review of the Current State of Knowledge and Perspectives, Rev. Geophys., 56, 409–453, https://doi.org/https://doi.org/10.1029/2017RG000593, 2018.

Gryspeerdt, E., Quaas, J., and Bellouin, N.: Constraining the aerosol influence on cloud fraction, J. Geophys. Res. Atmos., 121, 3566–3583, https://doi.org/https://doi.org/10.1002/2015JD023744, 2016.

Gryspeerdt, E., Goren, T., Sourdeval, O., Quaas, J., Mülmenstädt, J., Dipu, S., Unglaub, C., Gettelman, A., and Christensen, M.: Constraining the aerosol influence on cloud liquid water path, Atmos. Chem. Phys., 19, 5331–5347, https://doi.org/10.5194/acp-19-5331-2019, 2019.

Gryspeerdt, E., Mülmenstädt, J., Gettelman, A., Malavelle, F. F., Morrison, H., Neubauer, D., Partridge, D. G., Stier, P., Takemura, T., Wang, H., Wang, M., and Zhang, K.: Surprising similarities in model and observational aerosol radiative forcing estimates, Atmospheric Chemistry and Physics, 20, 613–623, https://doi.org/10.5194/acp-20-613-2020, 2020.

Gryspeerdt, E., Goren, T., and Smith, T. W. P.: Observing the timescales of aerosol–cloud interactions in snapshot satellite images, Atmospheric Chemistry and Physics, 21, 6093–6109, https://doi.org/10.5194/acp-21-6093-2021, 2021.

Heinze, R., Dipankar, A., Henken, C. C., Moseley, C., Sourdeval, O., Trömel, S., Xie, X., Adamidis, P., Ament, F., Baars, H., Barthlott, C., Behrendt, A., Blahak, U., Bley, S., Brdar, S., Brueck, M., Crewell, S., Deneke, H., Di Girolamo, P., Evaristo, R., Fischer, J., Frank, C., Friederichs, P., Göcke, T., Gorges, K., Hande, L., Hanke, M., Hansen, A., Hege, H.-C., Hoose, C., Jahns, T., Kalthoff, N., Klocke, D., Kneifel, S., Knippertz, P., Kuhn, A., van Laar, T., Macke, A., Maurer, V., Mayer, B., Meyer, C. I., Muppa, S. K., Neggers, R. A. J., Orlandi, E., Pantillon, F., Pospichal, B., Röber, N., Scheck, L., Seifert, A., Seifert, P., Senf, F., Siligam, P., Simmer, C., Steinke, S., Stevens,

https://doi.org/10.5194/egusphere-2025-5064
Preprint. Discussion started: 14 November 2025

B., Wapler, K., Weniger, M., Wulfmeyer, V., Zängl, G., Zhang, D., and Quaas, J.: Large-eddy simulations over Germany using ICON: a comprehensive evaluation, Q. J. R. Meteorol. Soc., 143, 69–100, https://doi.org/https://doi.org/10.1002/qj.2947, 2017.

Hill, A. A., Feingold, G., and Jiang, H.: The Influence of Entrainment and Mixing Assumption on Aerosol–Cloud Interactions in Marine Stratocumulus, Journal of the Atmospheric Sciences, 66, 1450 – 1464, https://doi.org/10.1175/2008JAS2909.1, 2009.

Keshtgar, B., Voigt, A., Hoose, C., Riemer, M., and Mayer, B.: Cloud-radiative impact on the dynamics and predictability of an idealized extratropical cyclone, Weather and Climate Dynamics, 4, 115–132, https://doi.org/10.5194/wcd-4-115-2023, 2023.

Lee, S. S., Penner, J. E., and Saleeby, S. M.: Aerosol effects on liquid-water path of thin stratocumulus clouds, Journal of Geophysical Research: Atmospheres, 114, https://doi.org/https://doi.org/10.1029/2008JD010513, 2009.

Lilly, D. K.: On the numerical simulation of buoyant convection, Tellus, 14, 148–172, https://doi.org/https://doi.org/10.1111/j.2153-3490.1962.tb00128.x, 1962.

Löhnert, U., Schween, J. H., Acquistapace, C., Ebell, K., Maahn, M., Barrera-Verdejo, M., Hirsikko, A., Bohn, B., Knaps, A., O'Connor, E., Simmer, C., Wahner, A., and Crewell, S.: JOYCE: Jülich Observatory for Cloud Evolution, Bull. Amer. Meteor. Soc., 96, 1157 – 1174, https://doi.org/10.1175/BAMS-D-14-00105.1, 2015.

Madhavan, B. L., Kalisch, J., and Macke, A.: Shortwave surface radiation network for observing small-scale cloud inhomogeneity fields, Atmos. Meas. Tech., 9, 1153–1166, https://doi.org/10.5194/amt-9-1153-2016, 2016.

Malavelle, F. F., Haywood, J. M., Jones, A., Gettelman, A., Clarisse, L., Bauduin, S., Allan, R. P., Karset, I. H. H., Kristjánsson, J. E., Oreopoulos, L., Cho, N., Lee, D., Bellouin, N., Boucher, O., Grosvenor, D. P., Carslaw, K. S., Dhomse, S., Mann, G. W., Schmidt, A., Coe, H., Hartley, M. E., Dalvi, M., Hill, A. A., Johnson, B. T., Johnson, C. E., Knight, J. R., O'Connor, F. M., Partridge, D. G., Stier, P., Myhre, G., Platnick, S., Stephens, G. L., Takahashi, H., and Thordarson, T.: Strong constraints on aerosol–cloud interactions from volcanic eruptions, Nature, 546, 485–491, https://doi.org/10.1038/nature22974, 2017.

Mülmenstädt, J. and Feingold, G.: The Radiative Forcing of Aerosol-Cloud Interactions in Liquid Clouds: Wrestling and Embracing Uncertainty, Curr. Clim. Chang. Rep., 4, 23–40, https://doi.org/10.1007/s40641-018-0089-y, 2018.

Mülmenstädt, J., Gryspeerdt, E., Dipu, S., Quaas, J., Ackerman, A. S., Fridlind, A. M., Tornow, F., Bauer, S. E., Gettelman, A., Ming, Y., Zheng, Y., Ma, P.-L., Wang, H., Zhang, K., Christensen, M. W., Varble, A. C., Leung, L. R., Liu, X., Neubauer, D., Partridge, D. G., Stier, P., and Takemura, T.: General circulation models simulate negative liquid water path–droplet number correlations, but anthropogenic aerosols still increase simulated liquid water path, Atmospheric Chemistry and Physics, 24, 7331–7345, https://doi.org/10.5194/acp-24-7331-2024, 2024a.

Mülmenstädt, J., Gryspeerdt, E., Dipu, S., Quaas, J., Ackerman, A. S., Fridlind, A. M., Tornow, F., Bauer, S. E., Gettelman, A., Ming, Y., Zheng, Y., Ma, P.-L., Wang, H., Zhang, K., Christensen, M. W., Varble, A. C., Leung, L. R., Liu, X., Neubauer, D., Partridge, D. G., Stier, P., and Takemura, T.: General circulation models simulate negative liquid water path–droplet number correlations, but anthropogenic aerosols still increase simulated liquid water path, Atmospheric Chemistry and Physics, 24, 7331–7345, https://doi.org/10.5194/acp-24-7331-2024, 2024b.

Possner, A., Eastman, R., Bender, F., and Glassmeier, F.: Deconvolution of boundary layer depth and aerosol constraints on cloud water path in subtropical stratocumulus decks, Atmospheric Chemistry and Physics, 20, 3609–3621, https://doi.org/10.5194/acp-20-3609-2020, 2020.

Quaas, J., Boucher, O., Bellouin, N., and Kinne, S.: Satellite-based estimate of the direct and indirect aerosol climate forcing, J. Geophys. Res. Atmos., 113, https://doi.org/https://doi.org/10.1029/2007JD008962, 2008.

https://doi.org/10.5194/egusphere-2025-5064
Preprint. Discussion started: 14 November 2025

Quaas, J., Arola, A., Cairns, B., Christensen, M., Deneke, H., Ekman, A. M. L., Feingold, G., Fridlind, A., Gryspeerdt, E., Hasekamp, O., Li, Z., Lipponen, A., Ma, P.-L., Mülmenstädt, J., Nenes, A., Penner, J. E., Rosenfeld, D., Schrödner, R., Sinclair, K., Sourdeval, O., Stier, P., Tesche, M., van Diedenhoven, B., and Wendisch, M.: Constraining the Twomey effect from satellite observations: issues and perspectives, Atmos. Chem. Phys., 20, 15 079–15 099, https://doi.org/10.5194/acp-20-15079-2020, 2020a.

Quaas, J., Arola, A., Cairns, B., Christensen, M., Deneke, H., Ekman, A. M. L., Feingold, G., Fridlind, A., Gryspeerdt, E., Hasekamp, O., Li, Z., Lipponen, A., Ma, P.-L., Mülmenstädt, J., Nenes, A., Penner, J. E., Rosenfeld, D., Schrödner, R., Sinclair, K., Sourdeval, O., Stier, P., Tesche, M., van Diedenhoven, B., and Wendisch, M.: Constraining the Twomey effect from satellite observations: issues and perspectives, Atmospheric Chemistry and Physics, 20, 15 079–15 099, https://doi.org/10.5194/acp-20-15079-2020, 2020b.

Quaas, J., Andrews, T., Bellouin, N., Block, K., Boucher, O., Ceppi, P., Dagan, G., Doktorowski, S., Eichholz, H. M., Forster, P., Goren, T., Gryspeerdt, E., Hodnebrog, , Jia, H., Kramer, R., Lange, C., Maycock, A. C., Mülmenstädt, J., Myhre, G., O'Connor, F. M., Pincus, R., Samset, B. H., Senf, F., Shine, K. P., Smith, C., Stjern, C. W., Takemura, T., Toll, V., and Wall, C. J.: Adjustments to Climate Perturbations—Mechanisms, Implications, Observational Constraints, AGU Advances, 5, e2023AV001 144, https://doi.org/https://doi.org/10.1029/2023AV001144, e2023AV001144 2023AV001144, 2024.

Seifert, A. and Beheng, K. D.: A two-moment cloud microphysics parameterization for mixed-phase clouds. Part 1: Model description, Meteorol. Atmos. Phys., 92, 45–66, https://doi.org/10.1007/s00703-005-0112-4, 2006.

Smalley, K. M., Lebsock, M. D., and Eastman, R.: Diurnal Patterns in the Observed Cloud Liquid Water Path Response to Droplet Number Perturbations, Geophysical Research Letters, 51, e2023GL107 323, https://doi.org/https://doi.org/10.1029/2023GL107323, e2023GL107323 2023GL107323, 2024.

Smith, S. J., van Aardenne, J., Klimont, Z., Andres, R. J., Volke, A., and Delgado Arias, S.: Anthropogenic sulfur dioxide emissions: 1850–2005, Atmospheric Chemistry and Physics, 11, 1101–1116, https://doi.org/10.5194/acp-11-1101-2011, 2011.

Toll, V., Christensen, M., Quaas, J., and Bellouin, N.: Weak average liquid-cloud-water response to anthropogenic aerosols, Nature, 572, 51–55, https://doi.org/10.1038/s41586-019-1423-9, 2019.

Twomey, S.: Pollution and the planetary albedo, Atmos. Environ., 8, 1251–1256, https://doi.org/https://doi.org/10.1016/0004-6981(74)90004-3, 1974.

Wang, H., Rasch, P. J., and Feingold, G.: Manipulating marine stratocumulus cloud amount and albedo: a process-modelling study of aerosol-cloud-precipitation interactions in response to injection of cloud condensation nuclei, Atmospheric Chemistry and Physics, 11, 4237–4249, https://doi.org/10.5194/acp-11-4237-2011, 2011.

Wang, S., Wang, Q., and Feingold, G.: Turbulence, Condensation, and Liquid Water Transport in Numerically Simulated Nonprecipitating Stratocumulus Clouds, Journal of the Atmospheric Sciences, 60, 262 – 278, https://doi.org/10.1175/1520-0469(2003)060<0262:TCALWT>2.0.CO;2, 2003.

Williams, A. S. and Igel, A. L.: Cloud Top Radiative Cooling Rate Drives Non-Precipitating Stratiform Cloud Responses to Aerosol Concentration, Geophysical Research Letters, 48, e2021GL094 740, https://doi.org/https://doi.org/10.1029/2021GL094740, e2021GL094740 2021GL094740, 2021.

Yanai, M., Esbensen, S., and Chu, J.-H.: Determination of Bulk Properties of Tropical Cloud Clusters from Large-Scale Heat and Moisture Budgets, Journal of Atmospheric Sciences, 30, 611 – 627, https://doi.org/10.1175/1520-0469(1973)030<0611:DOBPOT>2.0.CO;2, 1973.

Zängl, G., Reinert, D., Rṕodas, P., and Baldauf, M.: The ICON (ICOsahedral Non-hydrostatic) modelling framework of DWD and MPI-M: Description of the non-hydrostatic dynamical core, Q. J. R. Meteorol. Soc., 141, 563–579, https://doi.org/https://doi.org/10.1002/qj.2378, 2015.

https://doi.org/10.5194/egusphere-2025-5064
Preprint. Discussion started: 14 November 2025

Zhang, J., Zhou, X., Goren, T., and Feingold, G.: Albedo susceptibility of northeastern Pacific stratocumulus: the role of covarying meteorological conditions, Atmospheric Chemistry and Physics, 22, 861–880, https://doi.org/10.5194/acp-22-861-2022, 2022.

https://doi.org/10.5194/egusphere-2025-5064
Preprint. Discussion started: 14 November 2025

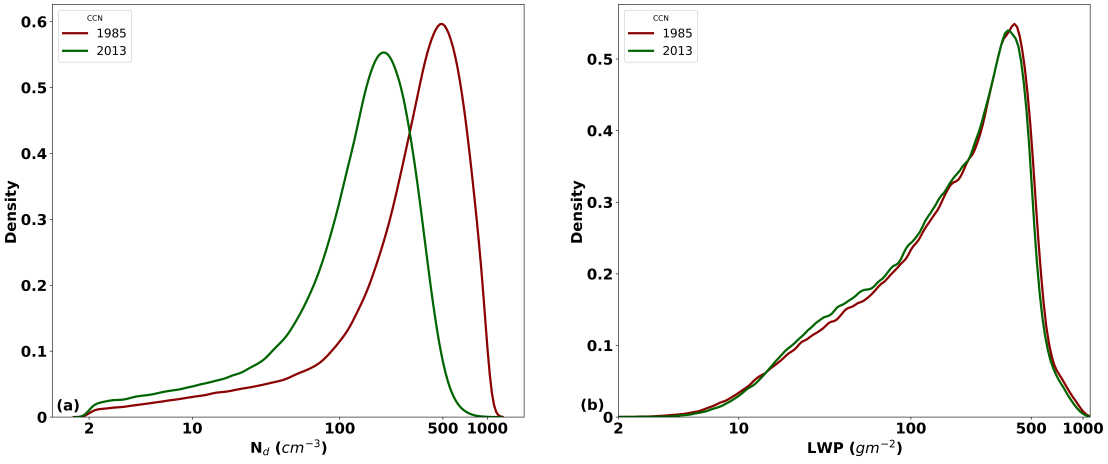

Figure 1. Comparison of (a) N_d (cm^{-3}) and (b) LWP (gm^{-2}) probability density function (PDF) for the 2103 and 1985 simulations. The green line represents the 2013 simulation, which uses the present-day (2013) CCN concentration, and the 1985 simulation uses the pre-induration CCN concentration (1985).

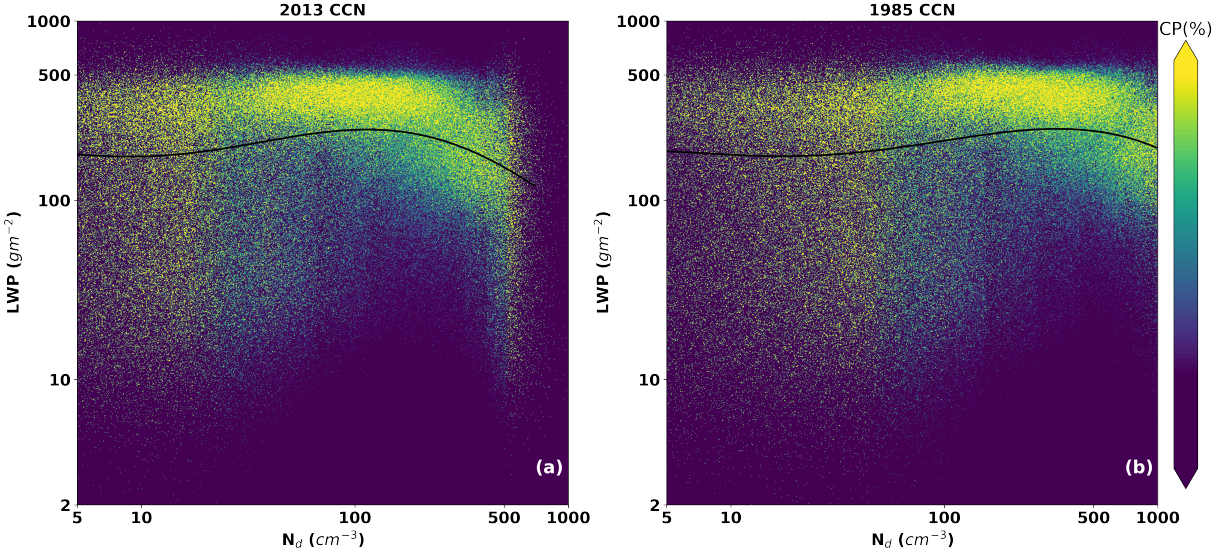

Figure 2. The N_d-LWP joint histogram for the (a) 2013 and (b) 1985 simulations. The thick black line in each plot shows the smoothed mean LWP ($\overline{\text{LWP}}$) at certain N_d bins (P (LWP | N_d)). CP(%) is condition probability: the probability of finding a certain LWP given certain N_d. The 2013 simulation uses present-day (2013) CCN concentration, and the 1985 simulation uses the pre-industrial (1985) CCN concentration.

https://doi.org/10.5194/egusphere-2025-5064
Preprint. Discussion started: 14 November 2025

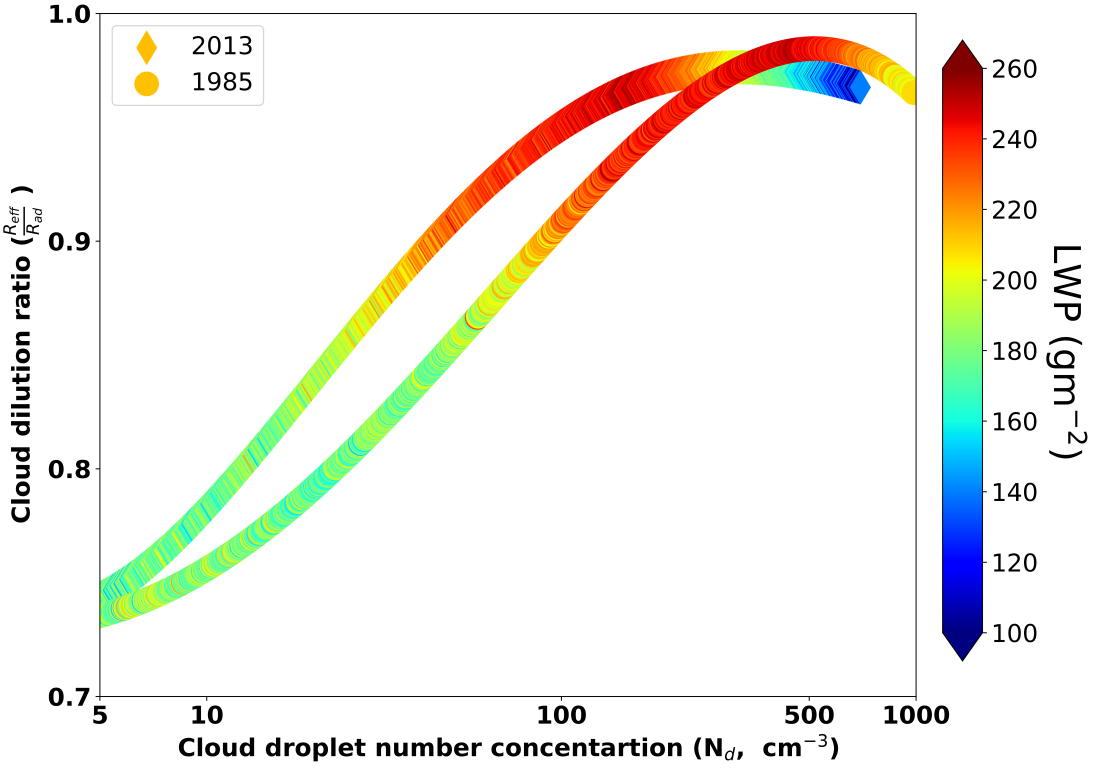

Figure 3. The N_d-bin mean cloud dilution ratio (ratio of $\overline{R_{eff}}$ to $\overline{R_{ad}}$) for the 2013 and 1985 simulations. The points represent the $\overline{R_{eff}}$ / $\overline{R_{ad}}$ at certain P (R_{eff} / R_{ad} | N_d). The diamond and the circle shape denote the 2103 and 1985 simulations, respectively.

https://doi.org/10.5194/egusphere-2025-5064
Preprint. Discussion started: 14 November 2025

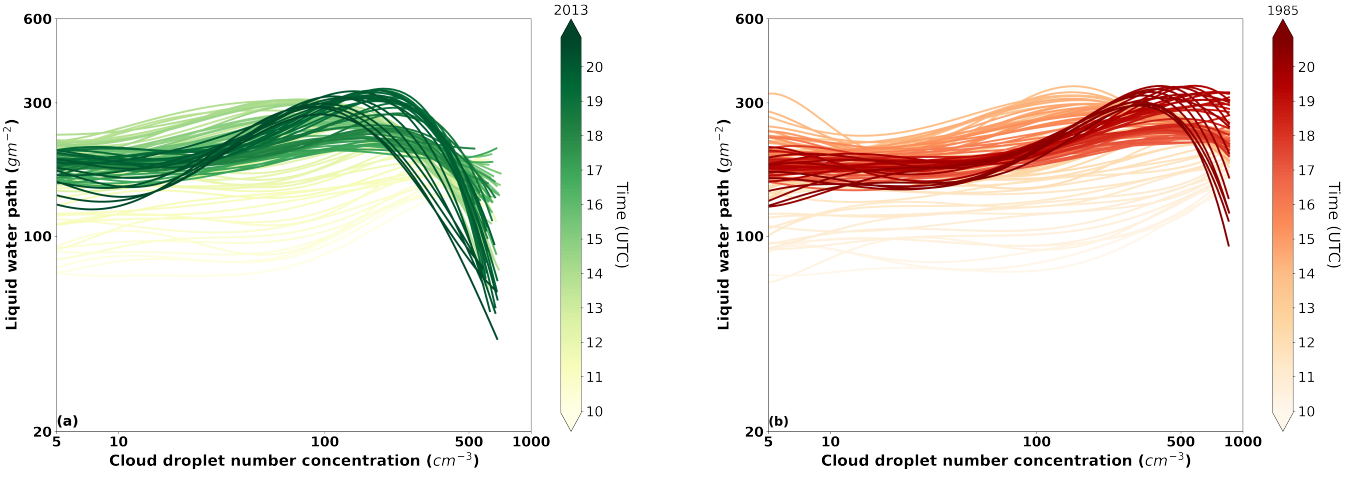

Figure 4. Temporal evolution of the mean LWP ($\overline{\text{LWP}}$) at certain N_d bins (P (LWP | N_d)) for (a) 2013 and (b) 1985 simulations. Each line indicates the N_d-LWP relationship at every model time step (5-minute interval), and the colour gradient indicates the Temporal evolution of the N_d-LWP relationship (from 1000UTC to 2000UTC).

https://doi.org/10.5194/egusphere-2025-5064
Preprint. Discussion started: 14 November 2025

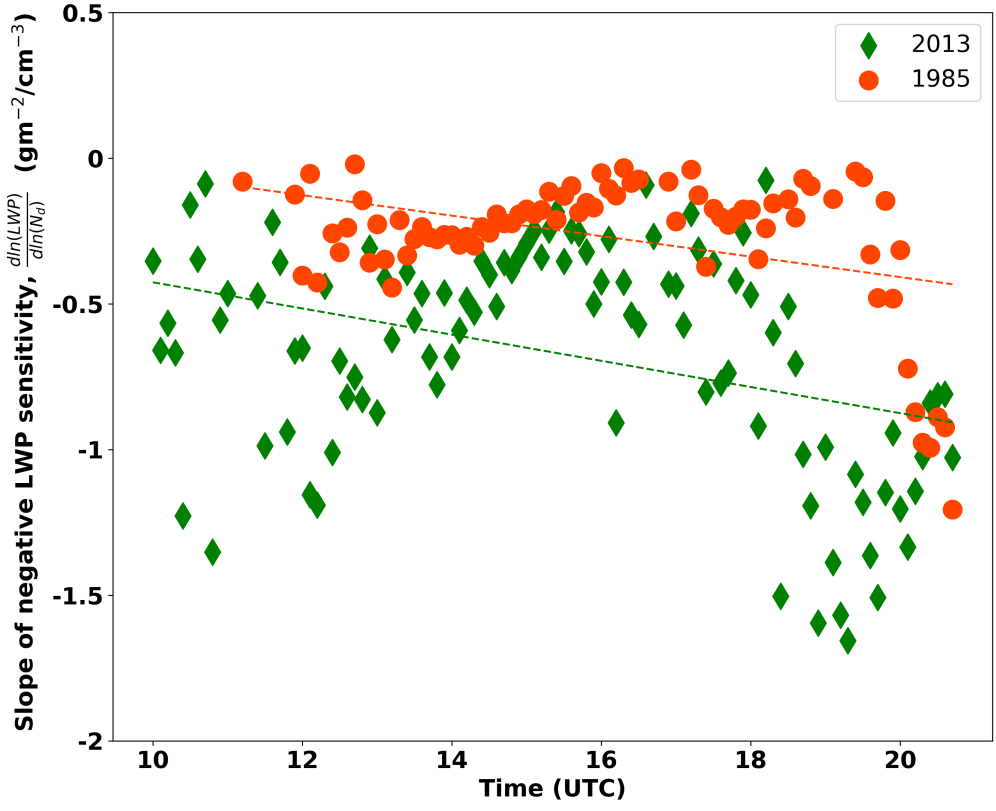

Figure 5. The magnitude of negative LWP (gm^{-2}) adjustment, as calculated by the N_d-LWP slope over time. The green diamond shape denote 2013 simulation, and the red circles denote the 1985 simulation. The respective dotted line indicates the linear regression.

https://doi.org/10.5194/egusphere-2025-5064
Preprint. Discussion started: 14 November 2025

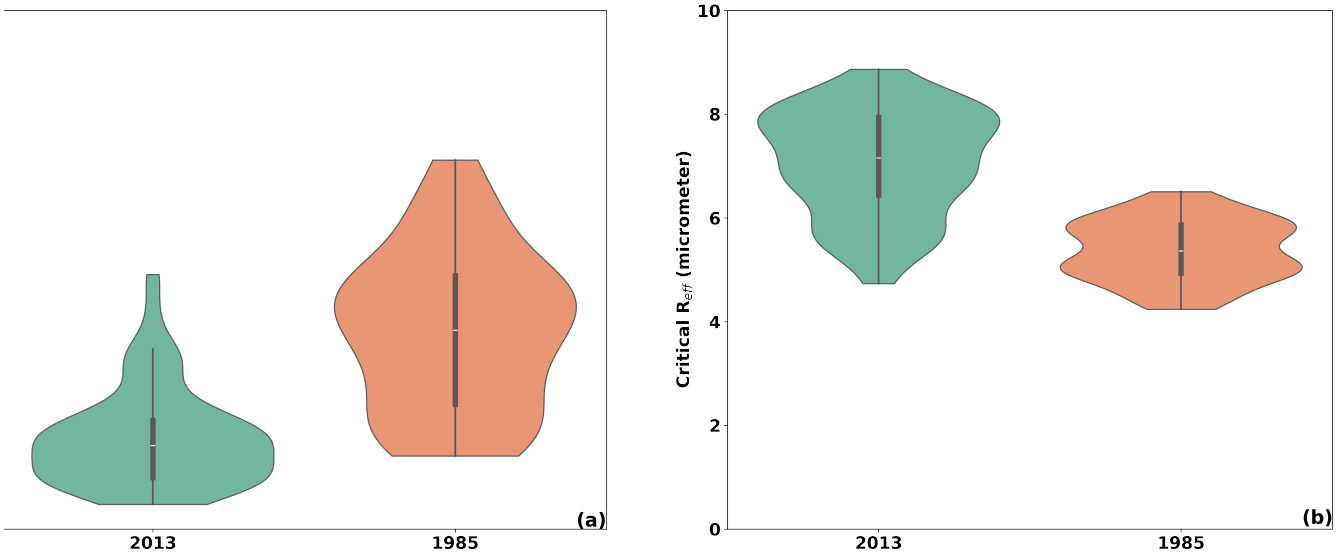

Figure 6. Violin plots for critical (a) N_d (cm^{-3}) and (b) R_{eff} (μ m). The critical indicates the N_d / R_{eff} at which the LWP adjustment becomes negative over time. The green colour denote 2013 simulation, and the red colour denotes the 1985 simulation. On each side, the grey line indicates the distribution shape of the data (PDF). The white dot on the violin plot represents the median, the back bar in the centre represents the interquartile range (first and third quartile), and the lower and upper parts of the violin plot represent the lower/upper adjacent values.

https://doi.org/10.5194/egusphere-2025-5064
Preprint. Discussion started: 14 November 2025

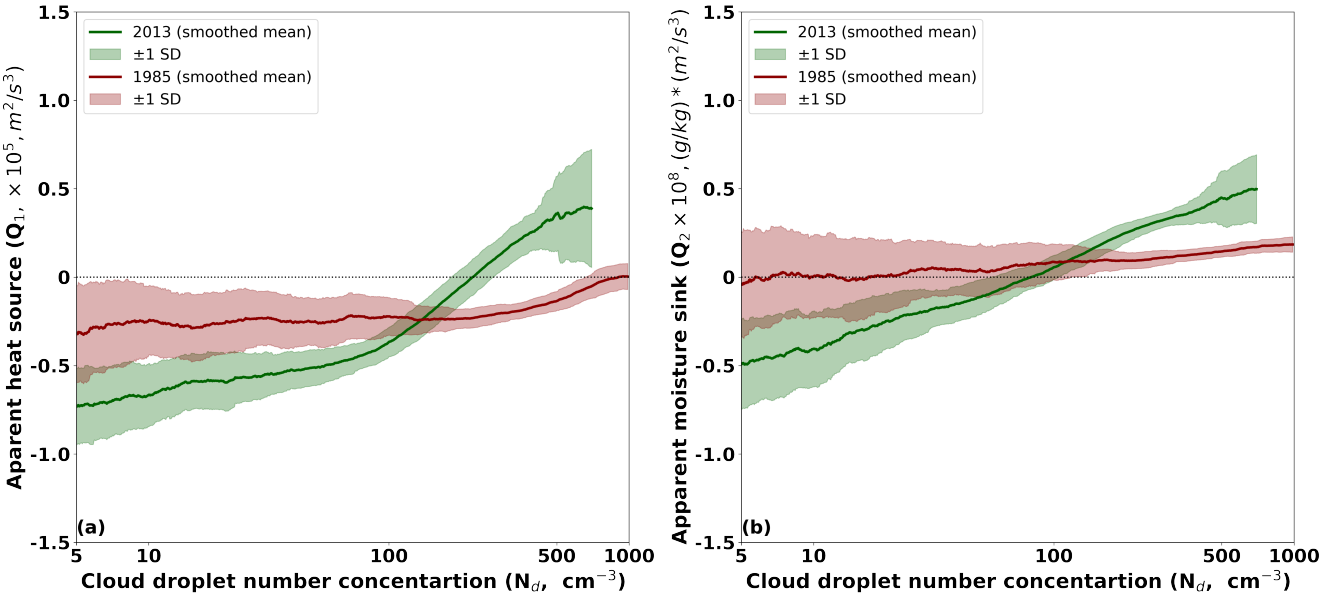

Figure 7. The Nd-bin mean (a) Q_1 and (b) Q_2 for the 2013 and 1985 simulations. The solid lines represent the smoothed mean of the mean Q_1 ($\overline{Q_1}$) and mean Q_2 ($\overline{Q_2}$) at certain N_d bins (same as Fig. 1). The shaded region represents the rolling standard deviation of the respective N_d-bin mean values. The solid green line represents the 2013 simulation, which uses present-day (2013) CCN concentration, and the solid red line represents the 1985 simulation, which uses the pre-induration CCN concentration (1985).

https://doi.org/10.5194/egusphere-2025-5064
Preprint. Discussion started: 14 November 2025

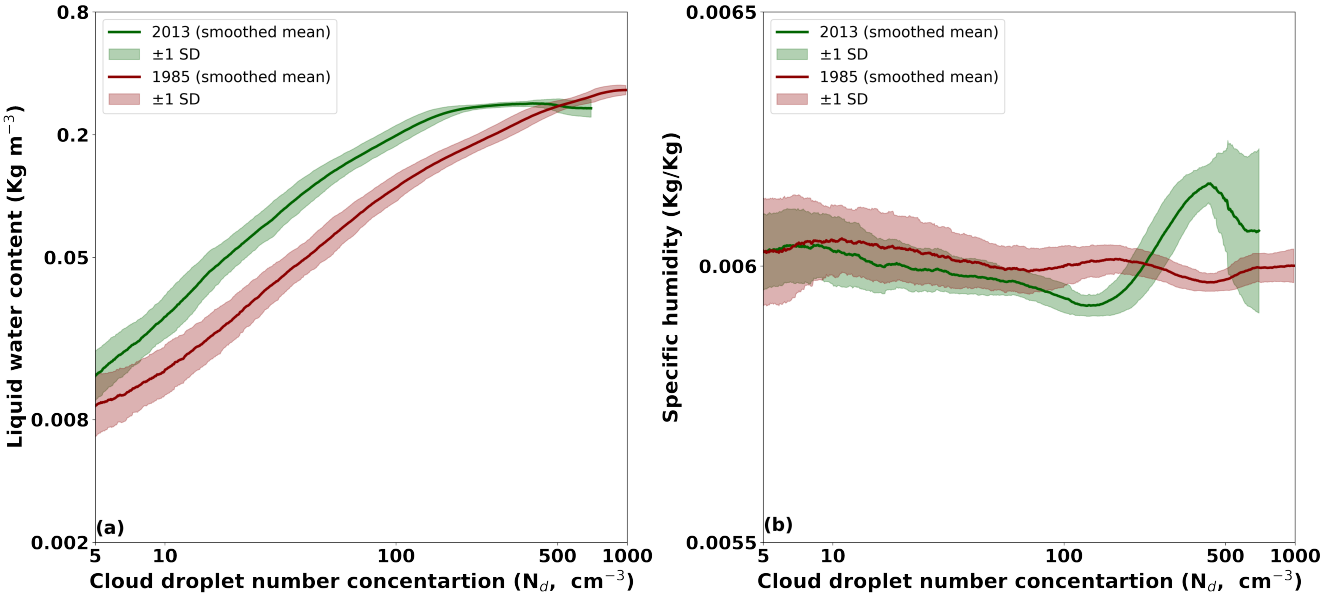

Figure A1. The N_d-bin mean (a) Liquid water content ($\overline{LWC}$) and (b) Specific humidity ($\overline{q_s}$) for the 2013 and 1985 simulations. The solid lines represent the smoothed mean of the mean LWC and specific humidity at certain Nd bins (same as Fig. 1). The shaded region represents the rolling standard deviation of the respective N_d-bin mean values. The solid green line represents the 2013 simulation, which uses present-day (2013) CCN concentration, and the 1985 simulation uses the pre-induration CCN concentration (1985).

https://doi.org/10.5194/egusphere-2025-5064
Preprint. Discussion started: 14 November 2025

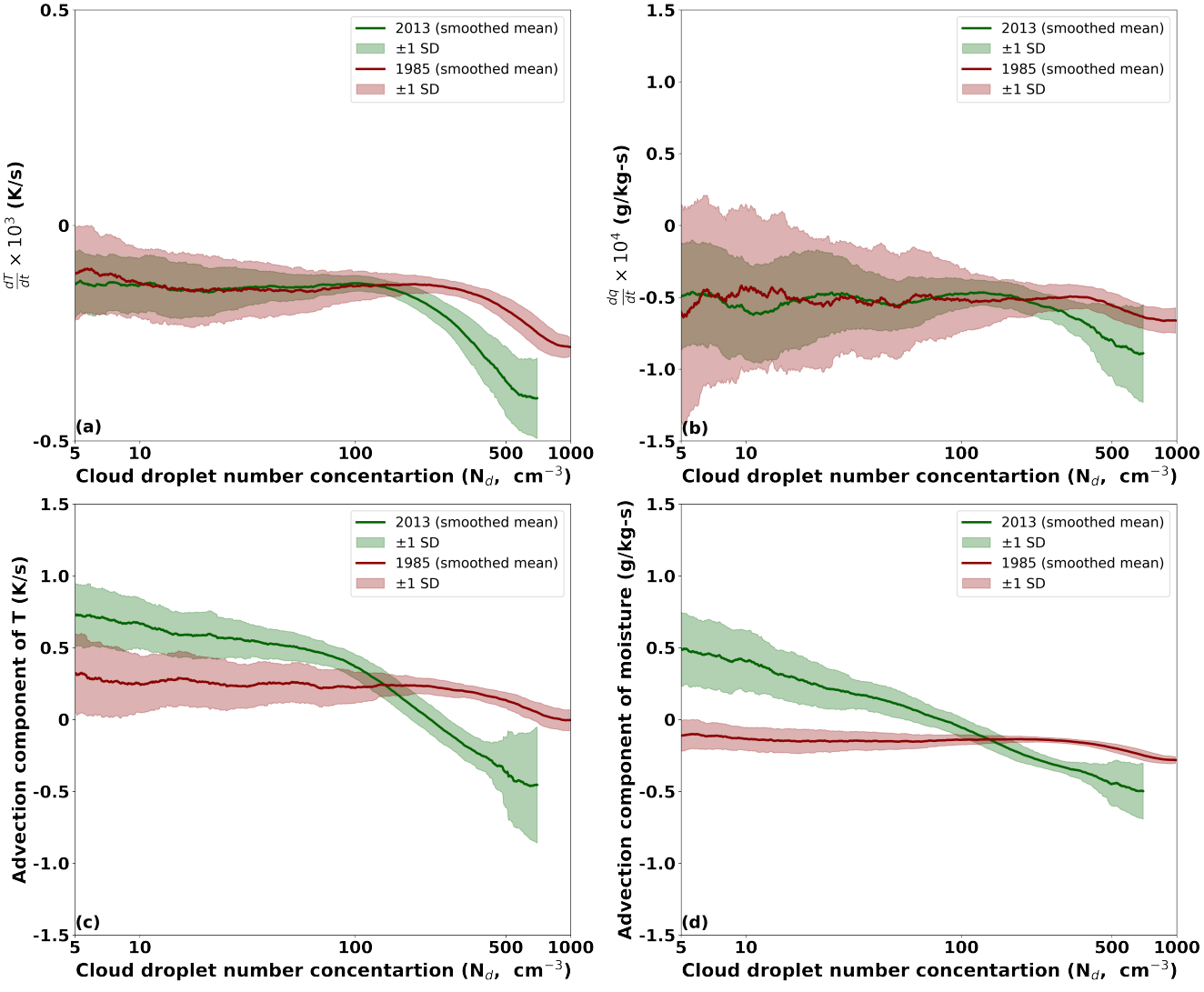

Figure A2. The N_d-bin mean (a) $\overline{\frac{dT}{dt}}$, (b) $\overline{\frac{dq}{dt}}$, (c) advection component of temperature, and (d)) advection component of moisture for the 2013 and 1985 simulations. The solid lines represent the smoothed mean of the mean values of the above variables at certain N_d bins (same as Fig. 1). The shaded region represents the rolling standard deviation of the respective N_d-bin mean values. The solid green line represents the 2013 simulation, which uses present-day (2013) CCN concentration, and the 1985 simulation uses the pre-induration CCN concentration (1985).